Exploring cocatalyst type effect on the Ziegler-Natta catalyzed ethylene polymerizations: experimental and DFT studies

Sergio Posada Pérez (sergio.posada@udg.edu)
University of Girona: Universitat de Girona https://orcid.org/0000-0003-4200-4264
Maryam Masoori
Iran Polymer and Petrochemical Institute, Tehran, Iran.
Mehdi Nekoomanesh
Iran Polymer and Petrochemical Institute, Tehran, Iran.
Reza Rashedi
Jam Petrochemical Company, Research and Development Department
Naeimeh Bahri
Iran Polymer and Petrochemical Institute, Tehran, Iran.

Research Article

Keywords: ethylene polymerization, Ziegler-Natta catalyst, polymerization kinetics, DFT simulations

Posted Date: February 3rd, 2022

DOI: https://doi.org/10.21203/rs.3.rs-1319165/v1

Exploring cocatalyst type effect on the Ziegler-Natta catalyzed ethylene polymerizations: experimental and DFT studies

Maryam Masoori[1], Mehdi Nekoomanesh[1], Sergio Posada-Pérez[2*], Reza Rashedi[3], Naeimeh Bahri Laleh[1*]

1. Department of Polymerization Engineering, Iran Polymer and Petrochemical Institute, Tehran, Iran. Email: n.bahri@ippi.ac.ir
2. Institut de Química Computacional i Catàlisi and Departament de Química, Universitat de Girona, c/ Maria Aurèlia Capmany 69, 17003 Girona, Catalonia, Spain. Email: sergio.posada@udg.edu
3. Bushehr, Asaluyeh, South Pars Special Economic Zone, Jam Petrochemical Company, Research and Development Department

Abstract

Due to the important role of cocatalyst in the polymerization process employing industrially favored Ziegler-Natta catalysts, its effect on kinetic behavior, catalyst activity, and polymer properties is discussed. In this paper triethyl aluminum (TEA) and triisobutyl aluminum (TIBA) have been used as the main cocatalyst ingredient with 10-20 mole percent of diethyl aluminum chloride (DEAC) and ethyl aluminum dichloride (EADC) cocatalysts. Among studied systems, neat TEA demonstrated the highest activity. Moreover, TEA-DEAC and TEA-EADC cocatalysts revealed a built-up kinetic profile, while TIBA-DEAC and TIBA-EADC show a decay-type kinetic curve. According to melt flow index results, no considerable change in flowability was detected in the synthesized polyethylenes (PE). On the other hand, the ethylene insertion and

chain termination mechanisms were scrutinized by means of density functional calculations using Ti active center located in (110) and (104) facets of the $MgCl_2$ surface. Results revealed that $TiCl_4$ supported (110) termination favors the PE chain production, being the ethylene insertion, the rate-determining step. To shed light on the bulkiness level of employed cocatalysts, buried volume (V_{Bur}) together with the two-dimensional map of cocatalyst molecules were considered. Higher V_{Bur} of TIBA can explain its lower activity and decay type kinetic profile obtained in the experimental section.

Keywords: ethylene polymerization, Ziegler-Natta catalyst, polymerization kinetics, DFT simulations

1. Introduction

Nowadays, it can be boldly said that the production of polymers using Ziegler-Natta catalysts is among the most important processes and has the largest portion in the production of plastics [1, 2]. Metallocene catalysts are nearly four decades old. Although advanced companies such as Basell, Dow, Sabic, Mitsui, Sommito, Borealis, Exxon Mobile, and Inoe use metallocene catalysts to produce some polyolefin grades, still more than 70 % of polyolefins are prepared by Ziegler-Natta type catalysts [3, 4]. It is well stablished that the first and most important parameter controlling the final polymer properties is the catalyst [5, 6]. On the other hand, it is noticed that the nature of this important chemical is practically undeniable without the presence of an activator known as cocatalyst [7, 8]. Many advances have been made in the catalysts structural studies and polymerization condition, although the effect of important factors such as electron donor, cocatalyst, and comonomer in the catalyst performance and polymerization process is not very well explored and understood [9]. Among these factors, cocatalyst, due to its primary role in switching the polymerization reaction, has relevant importance. In the past,

researchers believed that the cocatalyst is a passive component that only has the function of "removing impurity" and "alkylating" the active catalytic centers at the beginning of the polymerization, and then, does not play a specific role in the ongoing process. It has now been shown that the type of cocatalyst not only affects catalyst productivity but also alters the microstructure and arrangement of monomers in polymer chains during the polymerization reaction [10, 11]. In fact, after the catalyst, the selection of the appropriate cocatalyst is the most important and effective parameter in olefin polymerization processes [12]. Despite many studies on the catalyst structure, activity, polymerization, and properties of the polymer [13, 14], only a few investigations have been carried out on the reactions and interactions of cocatalyst [15, 16]. The process of cocatalyst interaction with Ziegler-Natta catalysts is well understood, but the performance of different types of cocatalyst in these interactions is still unclear [17, 18]. It is well-known that, in a polymerization process, the cocatalyst i) activates pre-catalyst particles, ii) participates in chain transfer reactions, iii) changes the isotacticity and molecular weight of the polymer [19], and iv) alters the kinetic stability and resistance to the decomposition of catalyst [20]. Notably, these functions by controlling catalyst performance, greatly alter the final properties of the produced polymer. Among the most common cocatalysts used in the commercial production of polyolefins are triethyl aluminum (TEA), triisobutyl aluminum (TIBA), diethyl aluminum chloride (DEAC), and ethyl aluminum dichloride (EADC). It is pointed out that such compounds, due to their various chemical structure, exhibit different behaviors in the olefin polymerizations. In fact, cocatalysts can form mono- and dimeric moieties, each one indicates different capabilities toward pre-catalyst reduction/activation [21]. In addition to the type of cocatalyst, their concentration plays a relevant role. Indeed, at lower cocatalyst concentrations, a large percentage of the primary catalyst remains inactive, and

impurities and toxins are not removed appropriately. As a result, the consumption of the catalyst increases dramatically, which is not economically affordable due to the high price of catalysts. Moreover, the high amount of cocatalyst (too optimal) causes excessive reduction of active catalytic centers and conversion of Ti^{3+} to Ti^{2+}, with the subsequent inactivation and deactivation in ethylene and propylene polymerizations, respectively. Owing to the fact that some cocatalysts have a positive effect on catalyst activity and others have a better ability to improve the product's properties, it has encouraged researchers to use a combination of cocatalysts [22]. Due to the industrial and academic importance of the topic, in this paper we thoroughly investigated the kinetics of catalyst behavior, and properties of the final polyethylene produced via a commercial $MgCl_2/TiCl_4$ based Ziegler-Natta catalyst in the presence of various cocatalysts including TEA, TIBA, and their combination with two chlorinated cocatalysts DEAC, EADC. Furthermore, molecular simulations by density functional (DFT) approach were employed to shed light on the polyethylene chain formation in different $MgCl_2$ lateral cuts and alkylating capability of employed cocatalysts.

2. Experimental

2.1. Materials

Hydrogen gas (purity >99%) as an active chain transfer agent was supplied from Roham Gas Company. An industrial $TiCl_4/MgCl_2$ based Ziegler-Natta catalyst, hexane as main medium in polymerization reactions, the polymerization grade of ethylene gas, were all acquired from Jam Company, Iran. Hexane was stored over a 4 Å activated molecular sieve. Triethylaluminium (TEA 1 M solution in hexane), triisobuthylaluminium (TIBA, 1 M solution in hexane), diethylaluminiumchloride (DEAC 1 M solution in hexane) and ethylaluminiumdichloride

(EADC 1 M solution in hexane) as cocatalysts were purchased from Merck, Germany, and used as received.

2.2. Ethylene polymerization

In this study, all the operations were carried out in dry and oxygen free media under nitrogen flow. Polymerizations were carried out in stainless-steel setup equipped with a mechanical stirrer, high-pressure injection system, a pressure, and a temperature sensor. In order to prepare the reactor for polymerization, the reactor was exposed to nitrogen for 1 h at 115 °C to remove impurities and moisture. After that, 650 mL of n-hexane was fed to the reactor at room temperature under nitrogen flow. After 3 min of degassing, the reactor was heated up to 80 °C, the 3 bar of hydrogen gas, 5 bar of ethylene gas, cocatalyst (with a different molar ratio of cocatalyst combination) and catalyst were injected into the reactor. After 2 h, the gases were completely vented, and the polymerization medium was cooled to room temperature. Finally, the polymer powder was dried at 85 °C.

2.3 Catalyst characterization

Scanning Electron Microscope (SEM): the catalyst morphology and distribution of elements on the surface of the catalyst was studied by SEM (VEGA TESCAN device made in Czechoslovakia) instrument. Inductively coupled plasma (ICP): The magnesium and titanium contents of the employed catalyst were determined by ICP. The power of the ICP spectrometer (Varian 710-ES) was 1.10 kW. The flow rates of plasma gas and auxiliary gas were 15.0 and 1.50 L min^{-1}, respectively. The pressure of nebulizing gas was 200 kPa and the pump speed was 13 rpm. Brunauer-Emmett-Teller (BET): Surface and pore analyses of the catalyst sample were done using the BET method (BELSORP Mini II). X-ray diffraction (XRD) of the catalyst was recorded using STOE-IPDS 2T diffractometer.

2.4 Polymer characterization

The melt flow index (MFI) of the synthesized polymers was measured using a Gottfert (MI-4) instrument. The polymer powders were mixed with 400 and 800 ppm of antioxidants (IRGANOX 1010, 168, respectively) before adding to the barrel. The MFI of powders was determined using ASTM D-1238 test method. The measurements were performed at 190 °C using 21.6, 5, and 2.16 kg loads, respectively.

2.5 Computational details

DFT calculations have been carried out with the Gausian16 [23] code using the BP86 functional of Becke and Perdew [24, 25], including corrections due to dispersion through the Grimme's method (GD3 keyword in Gaussian) [26]. The electronic configuration of the atoms has been described with the triple-ζ basis set with polarization of Ahlrichs for main-group atoms (def2-TZVP keyword in Gaussian) [27, 28]. The geometry optimizations were performed without symmetry constraints, and analytical frequency calculations confirmed the character of the located stationary points (only one negative frequency). These frequencies were used to calculate unscaled zero-point energies (ZPEs) as well.

3. Results and Discussion

3.1 Characterization of catalyst

In the study of catalyst and polymerization process, the most basic task is to identify the structure, components, configuration, size, and size distribution of the catalyst. With a basic knowledge of the structure and chemistry of a catalyst, a good prediction of the behavior of the catalyst in the polymerization process can be provided. Table 1 shows the results of the structure and properties of the catalyst.

Table 1. Characterization of employed commercial catalyst

Catalyst	Ti[a]	Mg[b]	Surf [c]	TPV[d]	APD[e]	D_avg[f]	X10	X50	X90
	2.4	13.3	243	0.241	3.97	42.8	3.2	41.5	85.8

a,b: weight percent (wt%), c: Surface area (m^2/g), d: Total Pore Volume (Cm^3/g), e: Average Pore Diameter (nm), f: Average dimension (µm)

According to the Table 1 results, the catalyst had a Ti content of 2.4 %, surface area of 243 m^2/g, average pore diameter of 3.97 nm and median particle size of 42.8 µm, which are accepted values for this class of systems. Furthermore, SEM picture, Figure 1, revealed completely spherical morphology of employed catalyst, which is beneficial to the powder conveying in the industrial gas-phase reactors. Elemental mapping analysis implied that apart from Mg and Cl atoms that are representative of $MgCl_2$ support, Ti atom is also present in the structure of the catalyst. Moreover, uniform dispersion of Ti atoms indicated well stablished homogeneously dispersion of active sites on the $MgCl_2$ support structure.

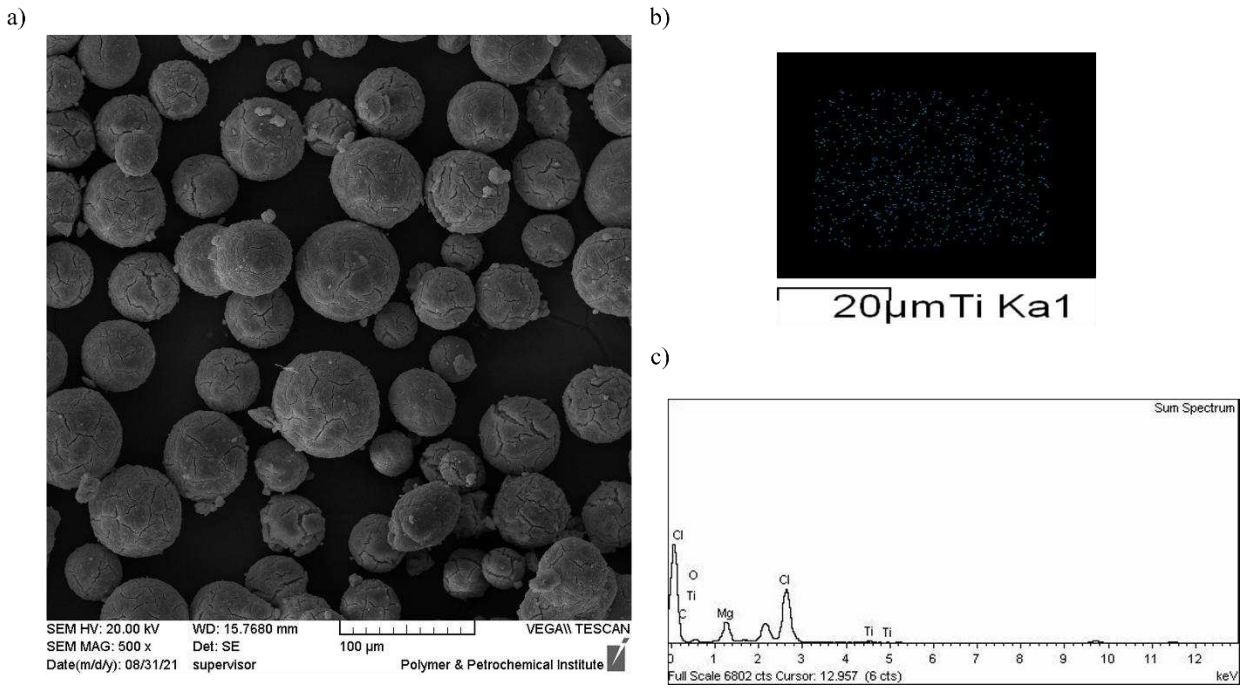

Figure 1. a) SEM, b) Ti map and c) EDX analyses of the employed catalyst

The XRD spectrum of the catalyst in 2θ angles between 5 and 65° is illustrated in Figure 2. In this pattern, the peaks at 2θ angles of 14° (stacking of Cl–Mg–Cl triple layers along the crystallographic direction), 33° (corresponded to (104) plane) and 50° (corresponded to (110) plane) were detected [29]. According to the literature, highly disordered catalyst is usually obtained by the rotational disorder of Cl-Mg-Cl triple layers, which subsequently lead to the formation of classically considered surfaces, i.e. (104) and (110) facets [6]. Therefore, in building molecular structure of a Ziegler-Natta catalyst, these surfaces should be considered.

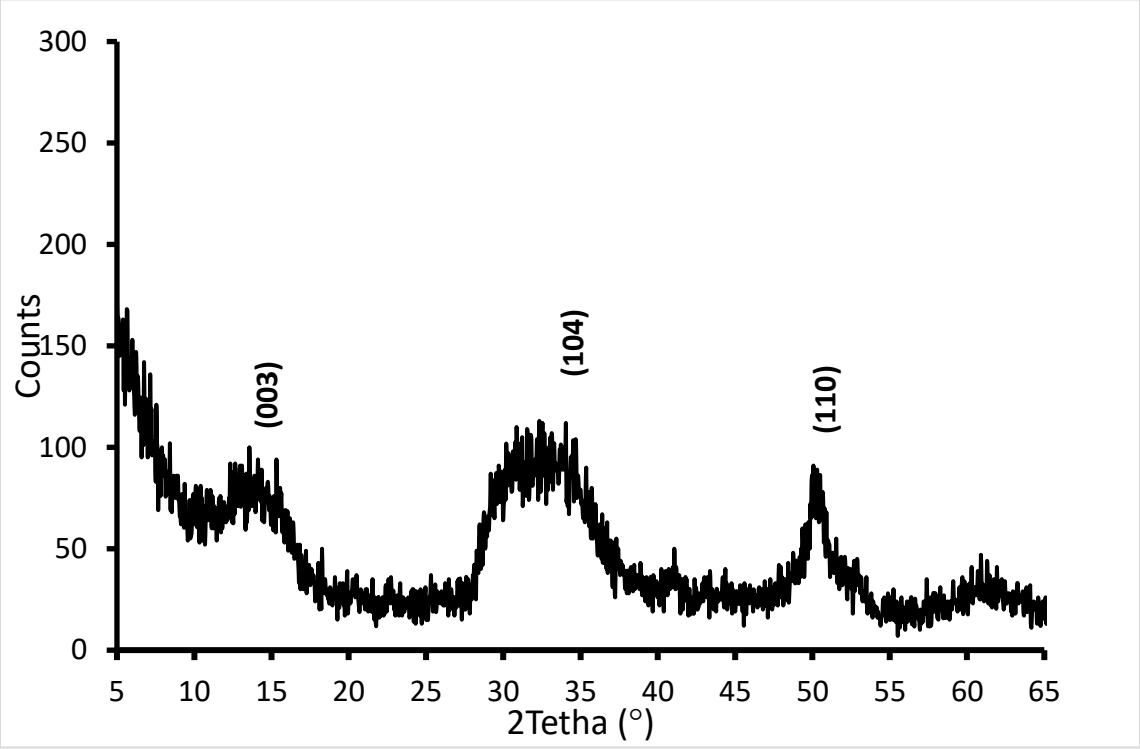

Figure 2. XRD pattern of the employed catalyst

3.2. Ethylene Polymerization in the presence of various cocatalysts

As mentioned, cocatalysts generally contain aluminum center, together with alkyl groups, chlorine atoms, etc., which based on their structure tune the performance of catalyst. Selecting the appropriate alkylaluminum can play a key role in the behavior of the catalyst, including polymerization activity, stereoselectivity, amount and distribution of active catalytic centers, as well as final characteristic of the polymer produced [4-8]. In this section, the polymerization behavior of employed Ziegler-Natta catalyst in the presence of various cocatalysts including TEA, TIBA, and TEA+DEAC, TEA+EADC, TIBA+DEAC, TIBA+EADC mixtures in different combinations of 90/10, 85/15, and 80/20, was surveyed in ethylene polymerization process.

For this purpose, in the constant molar ratio of Al/Ti = 200, the polymerization process was conducted in the presence of cocatalyst combinations under the same polymerization conditions. According to Table 2 results, catalyst activity was higher when TEA used as cocatalyst, in compare with TIBA. It can be attributed to the bulkiness of iso-buthyl groups which hinders its approaching to the Ti centers located in the interior parts of catalyst. By employing Cl containing Al complexes, EADC and DEAC, in the cocatalyst composition, the activity suppressed, however, no clear trend was found between the amount of Cl-containing cocatalyst and its type with the catalyst activity.

Table 2. Ethylene polymerization results using a variety of cocatalysts

Number of Runs	Cocatalyst type	Molar ratio of cocatalysts	Activity (kg polymer/g cat.h)	$MFI_{2.16}$ (g/10min)	MFI_5 (g/10min)	$MFI_{21.6}$ (g/10min)	FRR ($MFI_{21.6}$/ MFI_5)
1	TEA	100	4.25	1.046	3.065	29.575	9.64
2	TEA/DEAC	80/20	3	0.978	2.748	25.193	9.17

3	TEA/DEAC	85/15	3.25	1.060	3.016	27.455	9.1
4	TEA/DEAC	90/10	3.42	1.186	3.424	32.015	9.35
5	TEA/EADC	80/20	2.25	0.718	2.061	18.829	9.14
6	TEA/EADC	85/15	3	0.984	2.733	25.013	9.15
7	TEA/EADC	90/10	2.7	0.955	2.62	24.195	9.23
8	TIBA	100	3.33	1.999	3.213	29.386	9.2
9	TIBA/DEAC	80/20	2.51	1.097	2.996	26.68	8.9
10	TIBA/DEAC	85/15	2.22	1.009	2.813	24.818	8.8
11	TIBA/DEAC	90/10	3.04	1.203	3.307	28.844	8.7
12	TIBA/EADC	80/20	2.27	0.947	2.725	23.791	8.7
13	TIBA/EADC	85/15	3	1.297	3.666	32.206	8.8
14	TIBA/EADC	90/10	3.15	1.52	4.313	38.39	8.9

Polymerization conditions: P_{C2}: 5 bar, P_{H2}:3 bar, Al/Ti: 200, T: 80 °C, P_{tot}: 8.5 bar, t: 2 h, hexane: 650mL

In addition, the results of the Table 2 showed that the type of cocatalyst did not have a significant effect on the melt flow index. Although the polymers obtained in the presence of TIBA catalyst and TIBA/DEAC, TIBA/EADC compared to TEA and TEA/DEAC and TEA/EADC compounds had lower melt flow index and narrower FRR, this difference was not large enough to be considered. Therefore, it can be said that the type and amount of cocatalyst has not affected on the melt flow index.

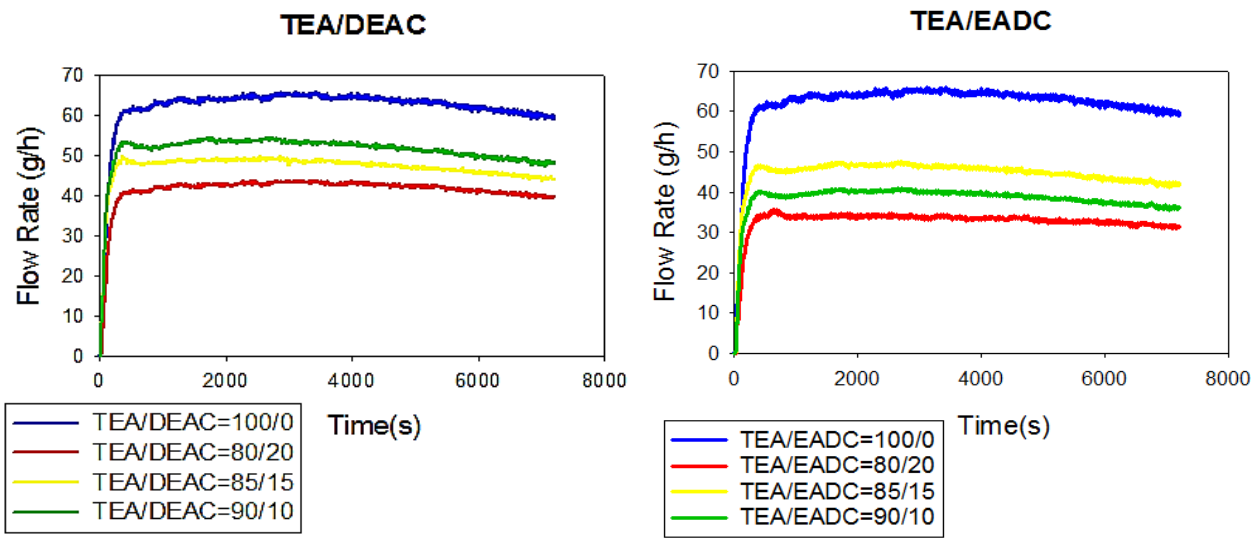

Figure 3. Rate-time profiles of ethylene polymerization with TEA, TEA+DEAC, TEA+EADC (Polymerization conditions: P_{C2}: 5 bar, P_{H2}:3 bar, Al/Ti: 200 mol/mol, T: 80°C, P_{tot}: 8.5 bar, t: 2 h, hexane: 650 mL)

Figure 3 shows the kinetic profiles of ethylene polymerization using TEA, TEA + DEAC, TEA + EADC cocatalysts under the same polymerization conditions. According to the diagrams, the polymerization kinetic in the presence of TEA, TEA+DEAC, TEA+EADC in three molar ratios of 90/10, 85/15, and 80/20 was build up type. In fact, the activity profiles in TEA, TEA + DEAC, TEA + EADC compositions were almost identical. It reveals that the presence of Cl-containing cocatalysts changed the absolute activity (area under the surface of curves), without alteration of activation and deactivation trend. It was corresponded to the lower molar ratio of Cl-containing cocatlysts (maximum 20 %) in the cocatalyst composition. Here, in line with activity results, TEA followed by TEA/DEAC (90/10) had the biggest area under the surface of kinetic curves.

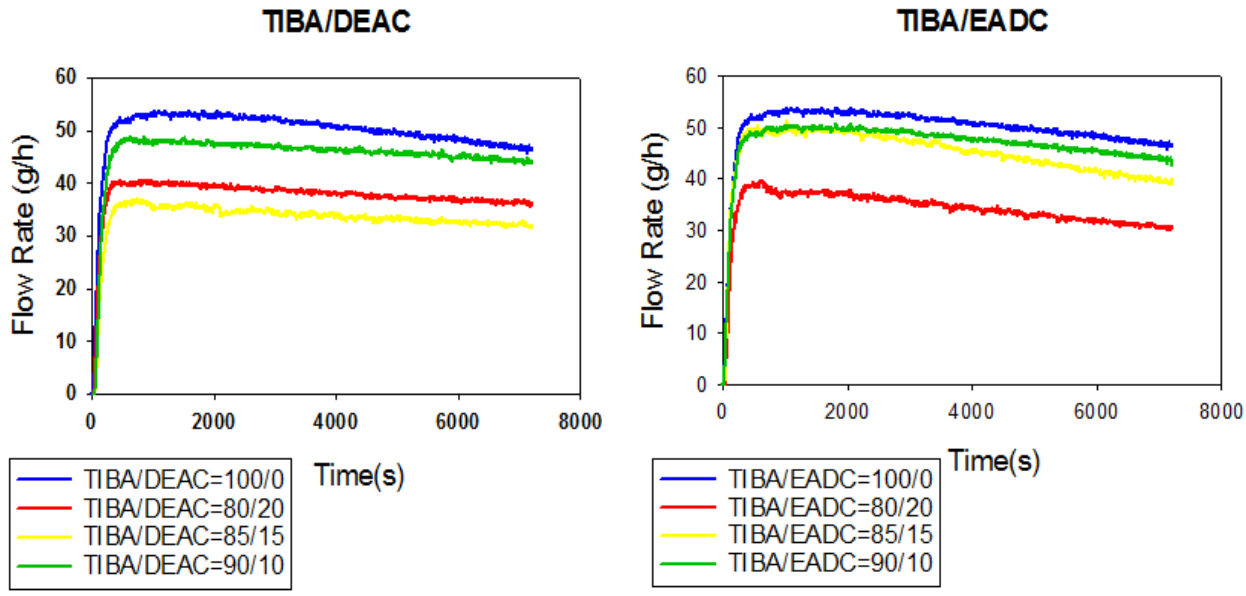

Figure 4. Rate-time profiles of ethylene polymerization with TIBA, TIBA +DEAC, TIBA +EADC (Polymerization conditions: P_{C2}: 5 bar, P_{H2}:3 bar, Al/Ti: 200 mol/mol, T: 80°C, P_{tot}: 8.5 bar, t: 2 h, hexane: 650 mL)

Figure 4. demonstrates the kinetics of ethylene polymerization in the presence of TIBA and its combination with DEAC and EADC in different ratios of 90/10, 85/15 and 80/20. By comparing Figures 3 and 4, it can be deduced that the polymerization kinetics in the presence of TEA containing compositions was almost build up, while in the presence of TIBA and related compositions, decay type polymerization behavior was identified. This can be attributed to the less bulkiness of TEA (will discussed as V_{Bur} term in the simulation section) which facilitates its effusion into the small cavities of catalysts where Ti centers were located. Therefore, it can be said that in an ethylene polymerization under the same condition, TEA compared to TIBA, due

to the small size of ethyl groups, will have a higher alkylation ability and consequently a higher polymerization rate.

3.3 Molecular modelling results

To elucidate the role of $MgCl_2$ surface on chain termination mechanism, DFT simulation has been performed. In particular, the (104) and (110) surfaces have been simulated, considering XRD pattern of employed catalyst which revealed domination of these lateral cuts. The catalytic pathway starts with the ethylene insertion and followed by the reaction with H_2 molecule, as the well-known chain transfer agent. In detail, the reaction mechanism is based on the neutral pentacoordinate species $TiCl_4Et$ **I** supported on $MgCl_2$ surface, where a thermodynamically favorable ethylene molecule is coordinated, forming the intermediate **II**. Then, the insertion of the olefin substrate in the Ti-C bond implies the first energy barrier, leading to, again, a pentacoordinate Ti specie (**III**). The following step implies the coordination of the hydrogen molecule to the resulting intermediate **III** leading to intermediate **IV**. Actually, this second substrate will allow the hydrogenation of the carbon attached to the titanium and at the same time the H transfer to the metal, forming the intermediate hydride **V**, together with the release of a butane molecule. Going to quantitative results, both surface terminations show practically the same energy barriers for the ethylene insertion and butyl formation as it is depicted in Figure 5. On (110) surface, the ethylene coordination was 2.3 kcal/mol favored than (104), although the energy barrier for the insertion into the Ti-C bond for (104) termination was 0.6 kcal/mol lower than for (110). The second energy barrier to consider is the H transfer from molecular H_2. As it is shown in Figure 5, the hydrogen transfer was not the rate determining step (rds) of the reaction on (110) surface, since the energy barrier was 9.9 kcal/mol, thus, 1.0 kcal/mol lower than the previous ethylene insertion. The transition state structure depicted on Figure 6a shows that butyl

molecule moves away from the Ti atom while one of the H atoms is bonded to Ti and the other forms the C-H bond with butyl. Similar mechanism was observed for (104) termination (see Figure 6b), although an energy barrier over than 45 kcal/mol was found, discarding *a priori* the H transfer reaction. Both transition state structures implied the bonding of both hydrogens on Ti as a previous step to eject and hydrogenate the butyl moiety. It has been observed that Ti atom supported on (104) move upwards during the proton transfer reaction, elongating the Ti-$Cl_{surface}$ bonds (~0.2 Å) and shortening the Ti-$Cl_{cluster}$ bonds (~0.1 Å) to accommodate protons and throw out the butyl moiety (see Figure 6b). Instead, the Ti-Cl bond elongation was not observed for (110) since the Ti atom did not change the initial position. This may explain the large energy difference found by DFT simulations.

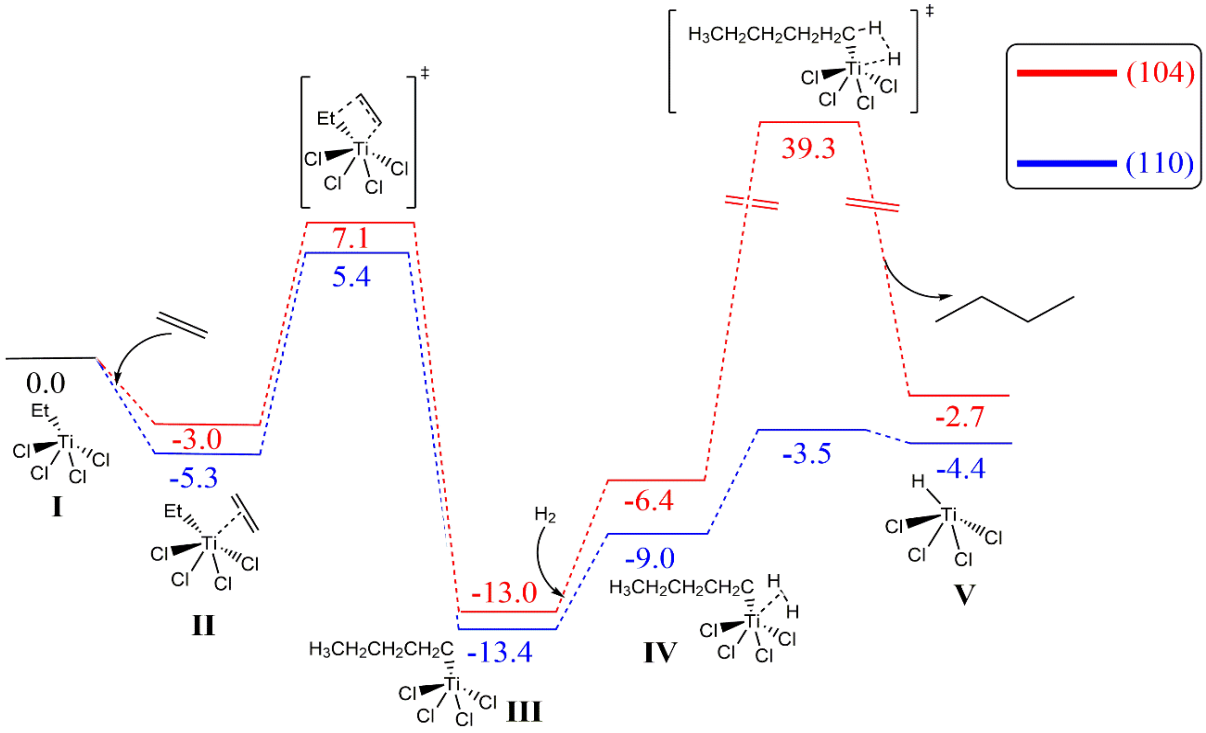

Figure 5. Reaction profile of ethylene insertion and proton transfer on $TiCl_4$ cluster supported on $MgCl_2$ (104) and (110) surfaces (relative Gibbs energies in kcal/mol).

a)

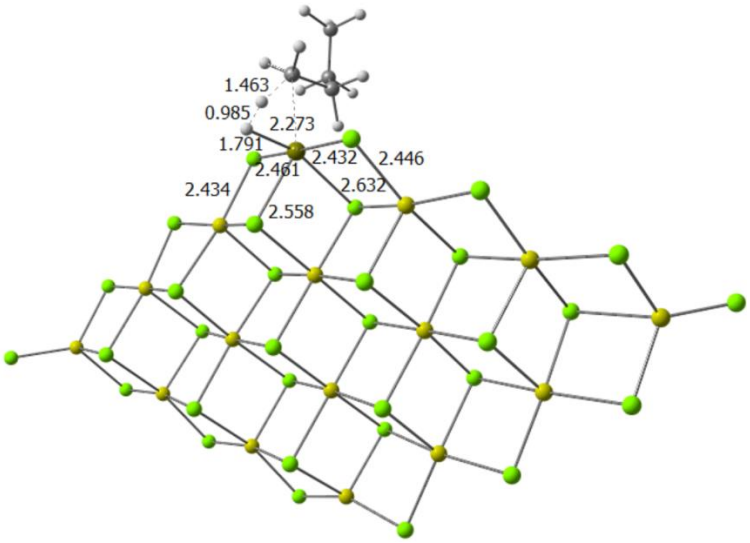

b)

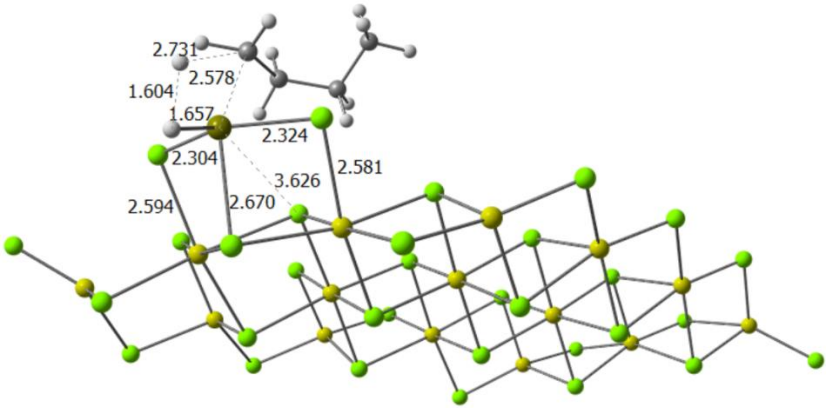

Figure 6. Transition state **IV-V** for a) (110) and b) (104) surfaces (selected distances given in Å).

According to literature, polymerization rate has a direct relationship with the formation of active centers through alkylation of $TiCl_4$ by the cocatalysts. As a result, each cocatalyst can play a major role in the rate of polymerization due to its unique chemical structure [19]. Considering that $TiCl_4$ catalysts supported on (110) termination is more catalytically active than on (104) cut, the effect of Al complexes in the transalkylation process to insert the ethyl on $TiCl_4$ clusters has been investigated. The structures have been optimized adsorbing the Al complex on chloride surface atom near to Ti site. The computed reaction energies suggested that the transalkylation is

thermodynamically favored using DEAC, by -5.8 kcal/mol Although the process using TEAL and EADC was endothermic, by 6.3 and 3.9 kcal/mol, respectively, the unfavorable thermodynamic energy values were relatively low, and thus, the reaction was still possible at room temperature. The use of the $\%V_{Bur}$ index, developed by Cavallo et al, [30] gives values of 78.7, 80,6, 74.6, and 76.2, for the TEA, TIBA, DEAC, and EADC, Al based systems, respectively [31]. Thus, the thermodynamic results are directly correlated with the sterical hindrance of the cocatalysts on the surface, and the steric maps in Figure 7 confirmed this hypothesis [32-34]. Indeed, when the steric hindrance increases, [35] the performance is worse [36, 37]. This fact could explain the lower activity of TIBA containing cocatalysts in comparison to TEA and the decay type of kinetic curves in the experimental section.

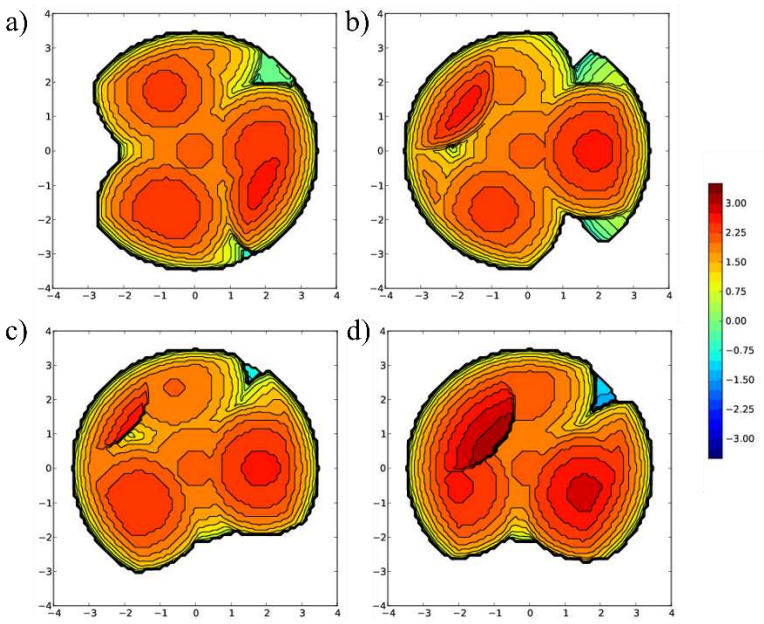

Figure 7. Steric maps (plane xy) of a) TEA b) TIBA, c) DEAC, and d) EADC with the linking a-C in the center, Ti in the z axis, and the b-C bonded to Ti on the XZ plane, of the TS **IV-V**, with a radius of 3.5 Å (for the Al based complexes Al was used as the center, the linking Cl in the z axis, and the closest a-C on the X axis).

Finally, the reaction mechanism was computed considering the most favorable cocatalysts according to experimental results (TEA) on (110) surface of $MgCl_2$. With the goal to explore the role of Cl-containing cocatalysts, the reaction mechanism with DEAC and EADC was investigated as well. To carry out these simulations, the Al complex was placed close to the Ti clusters and in top of chloride surface atom. Table 3 report the energy barriers for butyl formation (E_b 1) and proton transfer (E_b 2). In general, no huge variations on the rate limiting step of the reaction were found in comparison to the energy barriers calculated for the $TiCl_4$ cluster supported on $MgCl_2$ (110) surface. As it can be observed, TEA show the same energy value for the energy barriers, 11 kcal/mol. The DEAC cocatalysts show slightly lower energy barriers (1.4 kcal/mol) with respect to the use of TEA and the calculations without cocatalysts. Nevertheless, experimental results did not show an improvement of the catalytic activity combining DEAC (>20% molar concentration) with TEA. These results can be related with the low concentration of DEAC, which reduce the probability to be close to Ti sites. Therefore, our simulations suggest that the use DEAC as main cocatalyst would slightly improve the catalytic activity of the system. With respect to the EADC, the cocatalysts that contain more chloride ligands, presents the larger barriers. On the other hand, one can hypothesize that cocatalyst may play a most relevant role on $MgCl_2$ (104) termination, where the energy barrier is larger than 45 kcal/mol. The presence of cocatalyst may stabilize the Ti cluster, reducing the energy value of the rate limiting step.

Table 3. Gibbs energies (in kcal/mol) of the energy barriers on $MgCl_2$ (110) surface including the Al complexes

	E_b 1 (kcal/mol)	(kcal/mol) 2 $_bE$
Bare surface	10.9	9.9

TEA	10.9	11.0
DEAC	9.5	9.3
EADC	15.3	18.8

Conclusions

In this paper, effect of 14 kinds of cocatalyst compositions having different molar ratio of TEA, TIBA, DEAC and EADC on the catalytic performance of a commercial Ziegler-Natta catalyst was identified. In this regard, considering the molar composition of cocatalysts in industrial plants, TEA and TIBA were the main component, while DEAC and EADC were used in 10-20 molar percent. Among the studied cocatalyst compositions, TEA, TEA/DEAC (90/10) and TIBA revealed the largest activities, while no considerable effect on polymer MFI was detected. DFT simulations of a model Ziegler-Natta catalyst containing (110) and (104) surfaces unveiled the large energy barrier for the proton transfer process on (104) cut (45.7 kcal/mol) in comparison with the low energy barriers observed for (110) termination (11 kcal/mol, ethylene insertion). The $\%V_{Bur}$ show the higher free volume around TEA in compare with TIBA, confirming that steric hindrance problems of cocatalysts affects the catalytic activity. Finally, the reaction mechanism computed with TEA, DEAC, and EADC as cocatalyst, reveal that EADC is prejudicial due to the increase of the energy barriers, and DEAC slightly improve the catalytic activity.

Acknowledgements

S.P.P thank the Spanish Ministerio de Ciencia e Innovacion for Juan de la Cierva Formacion fellowship (FJC2019-039623-I).

Conflicts of interest

There are no conflicts to declare.

References

1. B. Jiang, X. Liu, Y. Weng, Z. Fu, A. He, Z. Fan, *J. Catal.*, 369, 324 (2019)
2. B. Jiang, Y. Weng, S. Zhang, Z. Zhang, Z. Fu, Z. Fan, *J. Catal.*, 360, 57 (2018)
3. M. A. Akram, X. Liu, B. Jiang, B. Zhang, A. Ali, Z. Fu, Z. Fan, *J. Macromol. Sci. A*, 58, 539 (2021)
4. N. Bahri-Laleh, A. Correa, S. Mehdipour-Ataei, H. Arabi, M. N. Haghighi, G. Zohuri, L. Cavallo, *Macromolecules*, 44, 778 (2011)
5. B. Jiang, B. Zhang, Y. Guo, A. Ali, W. Guo, Z. Fu, Z. Fan, *ChemCatChem*, 12, 5140 (2020)
6. N. Bahri-Laleh, A. Hanifpour, S. A. Mirmohammadi, A. Poater, M. Nekoomanesh-Haghighi, G. Talarico, L. Cavallo, *Prog. Polym. Sci.*, 84, 89 (2018)
7. B. Liu, Z. Tian, Y. Jin, N. Zhao, B. Liu, *Macromol. React. Eng.*, 12, 1700059 (2018)
8. E. Naji-Rad, M. Gimferrer, N. Bahri-Laleh, M. Nekoomanesh-Haghighi, R. Jamjah, A. Poater, *Catalysts*, 8, 224 (2018)
9. P. Li, Z. Fu, Z. Fan, *J. Appl. Polym. Sci.*, , 132, 28 (2015)
10. Y. Yu, T. F. L. McKenna, C. Boisson, M. S. Lacerda-Miranda, O. Martins, *ACS Catal.*, 10, 7216 (2020)
11. S. Gharajedaghi, Z. Mohamadnia, E. Ahmadi, M. Marefat, G. Pareras, S. Simon, A. Poater, N. Bahri-Laleh, *Mol. Catal*., 509, 111636 (2021)
12. J. Hu, B. Han, X. Shen, Z. Fu, Z. Fan, *Chinese J. Polym. Sci.*, 31, 583 (2013)
13. S. Rahmatiyan, N. Bahri-Laleh, A. Hanifpour, M. Nekoomanesh-Haghighi, *Polym. Int.*, 68, 94 (2019)
14. R. Bazvand, N. Bahri-Laleh, M. Nekoomanesh, H. Abedini, *Des. Monomers Polym.*, 18, 599 (2015)
15. E. S. Gnanakumar, R. R. Gowda, S. Kunjir, T. G. Ajithkumar, P. R. Rajamohanan, D. Chakraborty, C. S. Gopinath, *ACS Catal.*, 3, 303 (2013)
16. T. Wada, T. Funako, P. Chammingkwan, A. Thakur, A. Matta, M. Terano, T. Taniike, *J. Catal.*, 389, 525 (2020)
17. M. Fallah, N. Bahri-Laleh, K. Didehban, A. Poater, *Appl. Organomet. Chem.*, 34, e5333 (2020)
18. A. Thakur, P. Chammingkwan, T. Wada, R. Onishi, W. Kamimura, K. Seenivasan, M. Terano, T. Taniike *Appl. Cat. A: Gen*., 611, 117971 (2021)
19. P. M. Trivedi, V. K. Gupta, *J. Polym. Res.*, 28, 13 (2021)
20. N. Senso, P. Praserthdam, B. Jongsomjit, T. Taniike, M. Terano, *Polym. Bull.*, 67, 1979 (2011)
21. H. Trischler, W. Schöfberger, C. Paulik, *Macrom. React. Eng.*, 7, 146, (2013)
22. N. Senso N, S. Khaubunsongserm, B. Jongsomjit, P. Praserthdam, *Molecules*, 15, 9323 (2010)
23. M. J. Frisch GWT, H. B. Schlegel, G. E. Scuseria, M. A. Robb, J. R. Cheeseman, G. Scalmani, V. Barone, G. A. Petersson, H. Nakatsuji, X. Li, M. Caricato, A. V. Marenich, J. Bloino, B. G. Janesko, R. Gomperts, B. Mennucci, H. P. Hratchian, J. V. Ortiz, A. F. Izmaylov, J. L. Sonnenberg, D. Williams-Young, F. Ding, F. Lipparini, F. Egidi, J. Goings, B. Peng, A. Petrone, T. Henderson, D. Ranasinghe, V. G. Zakrzewski, J. Gao, N. Rega, G. Zheng, W. Liang, M. Hada, M. Ehara, K. Toyota, R. Fukuda, J. Hasegawa, M. Ishida, T. Nakajima, Y. Honda, O. Kitao, H. Nakai, T. Vreven, K. Throssell, J. A. J. Montgomery, J. E. Peralta, F.Ogliaro, M. J. Bearpark, J. J. Heyd, E. N. Brothers, K. N.Kudin, V. N. Staroverov, T. A.Keith, R. Kobayashi, J. Normand, K. Raghavachari, A. P. Rendell, J. C. Burant, S. S. Iyengar, J. Tomasi, M. Cossi, J. M. Millam, M.

Klene, C. Adamo, R. Cammi, J. W. Ochterski, R. L. Martin, K.Morokuma, O.Farkas, J. B.Foresman, D. J.Fox, (2016) Gaussian 16, Revision C.01, . Gaussian 16, Revision C01, Gaussian, Inc, Wallingford CT:
24. A, D, Becke, *Phys. Rev. A*, 38, 3098 (1988)
25. J. P. Perdew, *Phys. Rev. B*, 33, 8822 (1986)
26. S. Grimme, J. Antony, S. Ehrlich, H. Krieg, *J. Chem. Phys.*, 132, 154104 (2010)
27. F. Weigend, R. Ahlrichs, *Phys. Chem. Chem. Phys.*, 7, 3297 (2005)
28. F. Weigend, *Phys. Chem. Chem. Phys.*, 8, 1057 (2006)
29. N. Ghasemi Hamedani, H. Arabi, F. Poorsank, *New J. Chem.*, 44, 15758 (2020)
30. D. Pappalardo, C. Tedesco, C Pellecchia, *Eur. J. Inorg. Chem.*, 3, 621 (2002)
31. A. Poater, L. Cavallo, *Dalton Trans.*, 8885 (2009)
32. L. Falivene, R. Credendino, A. Poater, A. Petta, L. Serra, R. Oliva, V. Scarano, L. Cavallo, *Organometallics*, 35, 2286 (2016)
33. L. Falivene, Z. Cao, A. Petta, L. Serra, A. Poater, R. Oliva, V. Scarano, L. Cavallo, *Nat. Chem.*, 11, 872 (2019)
34. H. Jacobsen, A. Correa, A. Poater, C. Costabile, L. Cavallo, *Coord. Chem. Rev.*, 253, 687 (2008)
35. N. Bahri-Laleh, A. Poater, L. Cavallo, S. A. Mirmohammadi, *Dalton Trans.*, 43, 15143 (2014)
36. S. Kaur, V. Kumar, M. Chawla, L. Cavallo, A. Poater, N. Upadhyay, *Front. Chem.*, 5, 43 (2017)
37. M. Tomasini, J. Duran, S. Simon, L. M. Azofra, A. Poater, *Mol. Catal.*, 510, 111692 (2021)

Supplementary Files

This is a list of supplementary files associated with this preprint. Click to download.

- SIJIOPM.pdf